Section A-Research paper

FIBROUS Al_2O_3 POLYMER COMPOSITES CONTAINING NANOSIZED CeO_2 USED AS ADSORBENTS FOR ANTIMONY ION

Ngan Phan Thi Thu, Kohei Shimizu, Takaomi Kobayashi*

Department of Science of Technology Innovation, Nagaoka University of Technology, Nagaoka, 1603-1 Kamitomioka, Nagaoka, Niigata 940-2188, Japan.

Corresponding Author: T. Kobayashi (E-mail: takaomi@vos.nagaokaut.ac.jp)

ABSTRACT

Al_2O_3-polyethersulfone composite (APC) fiber prepared by wet-spinning method was used for deposition of CeO_2 on the fiber surface, when the fibers were immersed in aqueous $CeCl_3$ solution following by oxidation in H_2O_2 solution. The SEM-EDS analysis revealed that Ce was more highly deposited on the outer surface of the resultant CeO_2-Al_2O_3 composite fibers. The adsorbent behavior for the removal of antimony (Sb) was systematically examined, resulting in superior adsorption performance obeying Langmuir isotherm with maximum adsorption capacity of 7.71 mg/g, which was approximately 2.0 times higher than that of the non-deposited APC fiber. Additionally, in the fixed-bed column experiments for aqueous Sb solution, the CeO_2-deposited Al_2O_3 composite fibers performed their effectiveness in removing Sb from aqueous solutions in a continuous flow system.

Keywords: Fibrous antimony adsorbent, CeO_2-alumina composite fiber, Wet-spinning fibers, CeO_2 deposition, fixed-bed column

1. Introduction

Demand for rare metals has remarkably increased due to the development of advanced technologies, contributing to their expanding utilization of cutting-edge technologies. As of now, these rare metals are less distributed and produced only in limited areas, leading to a major

problem in securing their resources. Since advanced industrial nations producing such leading-edge products have almost no useful mineral resources, these countries rely on imports to produce almost all their rare earth resources. Also, the competition for mineral resources is intensifying as processed into high-tech products such as hybrid cars and electronic devices. Among such rare metals, antimony (Sb) serves as a crucial component in a variety of industrial sectors, including semiconductors for producing infrared detectors, diodes, and hall effect devices, the hardness of alloys in lead-acid batteries, small arms bullets, ceramics, and glass products [1–3]. However, major antimony producing countries are currently limited to China and Russia [4] and there are concerns about the restriction on its distribution. While antimony has the adverse effect of being toxic [5–7], its consumption is increasing with the development of flame retardants, lead-acid batteries, etc., as indicated by China Antimony Industry Report [8]. Therefore, technologies to recover such constrained resources have been received attentions in recent years, so-called urban mines, and their reuse is extremely important from the perspective of sustainable resource utilization, indicating the importance of Sb recovery from end-of-life products [9]. Thus, effective technologies for removal of Sb in aqueous solutions are very important to ensure environmental pollution control and human health, as well as valuable metal collection. Several methods for Antimony resource recovery were developed using coagulation or flocculation using metal oxides [10,11], oxidation reaction with Fe-Mn Binary oxide [12], and electrochemical removal process [13]. Some methods involve adsorption on resins [14] or activated carbon [15], but most involve adsorption on iron or other oxides [16] or their composites of chitosan [17] or Al_2O_3 [18]. Among them, although such cases were limited, cerium-doped powder materials on biochar [19], molecular sieve [20] and Fe_3O_4 magnetic particles [21] were reported in the presence of hydrous Al oxide clay minerals kaolinite [22] and

iron oxyhydroxides [23]. However, these powders and sediments having Sb adsorption ability have been reported to be obstructed in processing after adsorption. In fact, it is difficult to recover the powder-based initial adsorbents after adsorption, and a decrease in efficiency was reported even in continuous operation such as column separation [24,25]. It is desirable to adsorb and remove them on a carrier that can be easily separated. For the inconvenience of removing and recovering such adsorbents from the system, composite polymer scaffold could overcome their problem. For example, fibrous adsorbents having a large surface area allowed column separation with a low-pressure drop, making them beneficial for heavy metal removal [26]. Notably, zeolite polyethersulfone (PES)-composite fibers have been used for decontamination treatment, enabling the recovery of radioactive cesium [25]. Against this technological background, a fibrous adsorbent composited with alumina (Al_2O_3) was implemented for the development of new adsorption properties to fibrous adsorbents, showing effectiveness in the recovery of antimony. In this approach, a new adsorbent with a CeO_2 layer deposited on an Al_2O_3-polymer composite fiber was developed. The properties of CeO_2 deposited Al_2O_3-composited polyethersulfone (PES) fibers and their adsorption behavior towards antimony were investigated. In addition, continuous column adsorption experiments were conducted utilizing these fibers. For this purpose, such fibers containing CeO_2 or Al_2O_3 powders were fabricated by wet spinning method [26], and CeO_2 in the Al_2O_3 composite fiber was formed with H_2O_2 oxidative processing under various Ce^{3+} aqueous solutions [27] were used to investigate adsorption performance of Sb (III) from an aqueous solution in both batch and fixed-bed column experiments.

2. Experimental

2.1 Materials

Activated alumina KC-501 powder (Al_2O_3) was used without further treatments and purchased from Sumitomo Chemical Co. Ltd., Japan. Cerium (III) chloride heptahydrate was acquired from Sumitomo Chemical (Japan), and Cerium oxide powder (CeO_2) was supplied from Sigma-Aldrich. An oxidant solution of hydrogen peroxide (H_2O_2) with a concentration of 35 wt% was purchased from Tokyo Chemical Industry Co. Ltd. (Japan) and was utilized with aqueous form without further purification. Polyethersulfone (PES) was product of BASF Co. Ltd. (Germany), and *N*-methyl-2-pyrrolidone (NMP) from Nacalai Tesque Inc. Antimony (III) aqueous solution was prepared by diluting $SbCl_3$ (WAKO Pure Chemical Industry Co. Ltd.) for each concentration, and the pH of the solution was adjusted using 0.1 M HCl and 0.1 M NaOH solutions.

2.2 Preparation of CeO_2 deposited Al_2O_3 polymer composite fibers

Cerium oxide powder was directly dispersed into 30% of PES-NMP solution in 60% weight and then kept stirring for 24 h at room temperature, and then the mixed solution was extruded in water coagulation medium for the formation of PES in fibrous form as well as alumina PES composite fibers by phase inversion method through wet-spinning process. The similar approach was used in the case of alumina-PES composite (APC) fiber fabricated by phase inversion was on approach using wet spinning. Both PES and Al_2O_3 powder were mixed in the NMP and the mixture was stirred at room temperature for at least 12 hours before wet spinning process as previously reported [26]. Then the Al_2O_3-PES mixed solution was placed in a cylinder container with a hollow needle at the bottom and pressured at 0.3 MPa. The spinning of the solution squeezed it from the top of the needle to push into deionized water (5 L). The extruded NMP mixture dropped was instantly coagulated in the form of fiber into water, and the formed fibers

were left for a day in the water. After that, the fibers were washed at 80°C of hot water to remove residual NMP and finally, the Al_2O_3-PES composite (APC) fibers were dried under a vacuum.

To introduce cerium sites into composite fibers, the APC fiber was immersed in cerium aqueous solution and oxidized by H_2O_2 according to previous precipitation method [27] with modification. To prepare the Ce^{3+} aqueous solution, cerium (III) chloride heptahydrate was dissolved in deionized water at different concentrations ranging from 0.005 M – 0.1 M, as shown in Table 1. In 1000 ml of each solution, 30 g of APC fibers were cut into 30 cm length pieces and dispersed in the Ce aqueous solution, and stirred for 1 hour at 60°C. Then a certain amount of 3.5 wt% H_2O_2 solutions was dropped into the mixture solution. When the H_2O_2 solution was added, the solution color was changed immediately to bright orange from white, and the aqueous pH was adjusted to 6 by adding 0.5 M NaOH solution. The CeO_2-deposited composite fibers were then agitated for 24 hours by shaking in 500 ml of deionized water. Lastly, the composite fibers were dried in the oven at 60°C for 1 day.

2.3 Characterization of cerium oxide deposited APC fibers

The morphology of their composite fibers was observed using a scanning electron microscope (SEM) with an energy dispersive spectrometer (EDS) (JSM-5300LV; JEOL Ltd., Japan). X-ray diffractometer (Smart Lab, Rigaku, Japan) (XRD) was used to confirm the inorganic components like Al_2O_3 and CeO_2 in the fibers, when Cu-K_α radiation (λ = 1.54056Å) was at 40 kV and 30 mA. The XRD patterns were recorded in the 2θ range from 10° to 80° and the scanning speed was 2°/min. The Bruner-Emmett-Teller (BET) surface area and the BJH pore size distribution of composite fibers were measured with a nitrogen gas adsorption instrument (TriStar II 3020; Micromeritics Instrument Corp., USA) at 77K. The CeO_2 content was measured using X-ray fluorescence (XRF) instrument (ZSX Primus II; Rigaku Corp., Japan). Zeta potential of the

composite fibers was measured at several pHs using a Zeta-potential analyzer (ELSE1NGK; Otsuka Electronics Co. Ltd., Japan). The mechanical properties of the composite fibers for tensile strength were measured using LTS-500 N-S20 (Minebea, Japan) with a crosshead speed of 1.5 mm/s and a gauge length of 30 mm. Each specimen was 50 mm in length. The diameter of each sample was measured using a micrometer to calculate the area of a cross-sectional surface. Five specimens were tested for each sample. The values of tensile strength were calculated using the equations; Tensile strength (N/mm^2) = maximum load/ cross-sectional area (1). The value of density $\rho\ (\frac{g}{cm^3}) = \frac{W_s}{W_s - W_w} \times (\rho_o - d) + d$ (2), where W_s was the specimen weight in the air (g), W_w represented the specimen mass in methanol (g), ρ_o was the density of methanol (g/cm^3) at 20^oC and d was the density of air (g/cm^3) at 20^oC.

2.4 Adsorption experiment of Antimony (Sb)

Batch adsorption experiments were carried out by following, when the fiber was immersed in the aqueous Sb solution. Then, for determining the Sb concentration remaining in the aqueous Sb supernatant Inductively Coupled Plasma – Optical Emission Spectroscopy (ICP-OES) (Varian 720-ES; Varian Inc., Ca, USA) was operated. The amount of antimony adsorbed on the fibers was estimated from the decrease of antimony concentration when the composite fiber was soaked in the aqueous antimony solution. On the analysis process, standard stock solution (1000 mg/L) was prepared from $SbCl_3$ in deionized water and was diluted to the desired concentration from their stock standard solution. Here, the pH was adjusted to pH 6 when 0.1 M HCl and 0.1 M NaOH solutions were used. The composite fibers (0.1 g) were cut into approximately 2 cm length pieces and were added to 50 mL of the Sb solution in cases of each batch adsorption test under shaken process at room temperature. Then the fibers were filtered with a membrane filter having 0.45 μm of pore size as the testing times were reached. In remaining supernatant Sb

concentration, the uptake amount of Sb to the composite fibers was calculated by the following equation: $q = \frac{(C_i - C)V}{m}$(3), where q was the amount of Sb adsorbed (mg/g), m was the weight of the adsorbents (g), C_i and C were the initial and final concentration of the Sb in the solution (mg/L), and V represents the volume of the solutions (L).

For the adsorption experiments in column flow system, a polyvinyl chloride cylindrical (PVC) tube with an inner diameter of 1.3 cm and a length ranging from 10 to 30 cm was utilized. The tube was packed with fibers to achieve a fixed packing density of 30%. The fixed packing density was determined according to previous method [24]. The Sb feed solution continuously flowed into the packed column in an upward direction at flow rate of 2.5, and 5 mL/min using a peristaltic pump. Effluent samples were collected from the top of the columns at different predetermined time intervals, and the concentration of Sb residual ion concentration was measured using ICP-OES as well as the batch adsorption test. In the column experiment, various conditions in the column height, the flow rate, and the initial concentration of Sb were applied. The performance of column adsorption was analyzed using dynamic adsorption models named Adams-Bohart.

3. Results and discussion

3.1 Characterization of composite fibers deposited with CeO_2

After wet spinning for APC fiber, aqueous $CeCl_3$ with 0.005M, 0.01M, 0.05M and 0.1M was prepared and the fiber was immersed under H_2O_2 oxidation. Then, the obtained fibers were named APC-Ce 0.005, APC-Ce 0.01, APC-Ce 0.05, and APC-Ce 0.1 to each other in their respective concentrations, respectively. Figure 1 showed SEM-EDS morphology for each fiber at 200× for the cross section and 100× for surface of the fibers. As seen, the round cross-section of

each fiber was observed at about 500 μm in diameter. The PES-CeO2 was PES fiber mixed with 60 wt% CeO2 powder 150 in the NMP solution for the wet spinning process. Here, EDS views with yellow points indicated the presence of Ce species in the fiber. Apparently, the yellow points for the Ce distribution were high in the case of the PES-CeO_2 fiber throughout the fiber cross-section. Relative to this, the color point number cases of the APC-Ce fibers, which was in the post-oxidative for CeO_2 deposition, the deposition of Ce gradually increased when the $CeCl_3$ concentration was increased for the treatment of the APC fiber. Especially at 0.1M concentration of $CeCl_3$, the fiber surface of the APC-Ce 0.1 fiber had higher Ce distribution rather than inside of the fiber, meaning that the Ce oxidation occurred mostly on the outer surface. This indicated that the amount of Ce deposited on the APC composite fiber was depended on the dose-distribution of Ce solution. By using XRF analysis, the Ce content (wt%) in the APC-Ce 0.1 was 2.27 %, while the contents of APC-Ce 0.005 were extremely lower at 0.78%, which was summaried in Table 1.

Figure 2 compares XRD patterns of the resulting fibers, depicting Al_2O_3-PES fibers immersed in various Ce^{3+} concentrations and then H_2O_2 oxidation. The figure includes results for Al_2O_3, PES, and CeO_2 mixtures. The peaks attributed to χ-Al_2O_3 were observed at 2θ values of 37.3, 42.6, and 67.0 deg, as shown by closed circle symbols. Each peak was supported by a PDF card number: 00-013-037. The CeO_2-Al_2O_3 and CeO_2-Al_2O_3 mixture curves had three corresponding peaks of CeO_2 at 2θ values of 28.6, 47.5, and 56.3 deg, as indicated with PDF card number 01-075-947 [27]. Here, the CeO_2 peak is shown with closed triangle symbols. Relative to Al_2O_3 peaks, the weaker CeO_2 could overlap at same angles of Al_2O_3. These results demonstrated that the CeO_2 contents were increased when the increase of the Ce^{3+} concentration in the preparations of 0.005 – 0.1 M.

Table 1 also contained the density and tensile strength of the composite fibers. The fiber density of PES was 0.79 cm^3/g, and the value of the tensile strength was 9.5 MPa. Compared to PES-CeO_2 fiber, the density was almost the same, but the mechanical strength of the fiber was slightly stronger with the addition of CeO_2. When Al_2O_3 was added, the mechanical strength of the fiber was similar to that of PES fiber, but the density of APC fiber was doubled relatively to that of PES. The increase in density by adding Al_2O_3 to PES was attributed to the porous nature of Al_2O_3 [28]. On the other hand, when post-oxidized with H_2O_2, the fiber strength slightly decreased with increasing Ce^{3+} concentration. It was apparent that the density was slightly decreased with increasing the Ce contents in the fibers. This meant that the deposited CeO_2 embedded the space of Al_2O_3 powders in the fibers.

Figure 3 showed a) N_2 adsorption isotherm and b) BJH pore distribution of each fiber. According to the IUPAC classification, all of the fiber samples exhibited type-IV isotherm meaning typical mesoporous fashion [28]. In contrast to these, the PES-CeO_2 fiber belonged to type II isotherms [29], indicating the absence of Al_2O_3 having macroporous structures within the fiber. As presented in b), the BET results of the Ce-deposited APC fibers obtained sorption data through the Barret-Joyner-Helene (BJH) model. The result indicated that the APC fiber and the CeO_2-deposited APC fibers had pore size peaks of about 6 nm, corresponding to the alumina pore size, suggesting that no blocking the Al_2O_3 mesoporous with CeO_2 precipitation was formed. As shown in Table 1, the surface area of PES fiber was 58.8 m^2/g, and that of APC fiber was 96.1 m^2/g, meaning that the Al_2O_3 introduction to the composite fiber created higher porous properties. Nevertheless, when the H_2O_2-oxidative process was finished, the deposited CeO_2 on the surface of the APC fiber increased the surface area slightly, as it changed from 96.1 of APC fiber to 103.1 m^2/g of the APC-Ce 0.005. However, when the Ce^{3+} solutions were changed from 0.01 to

0.1 M, the value of the BET surface area of APC-Ce 0.01 and APC-Ce 0.1 were decreased from 99.6 to 95.6 m^2/g, respectively. As seen in EDS images, the CeO_2 deposition was mainly on the surface of the fibers. Therefore, the deposited CeO_2 remained in the Al_2O_3 meso-porous space after the post-oxidation process.

3.2 Sb adsorption behavior of fiber adsorbents having CeO_2

Figures 4 show (a) time dependence of adsorption amounts of Sb (III) and (b) adsorption isotherm of Sb for their fibers. The amounts q_t increased within 12 hours and then still gradually increased to be almost constant at about 48 hours, indicating saturation binding. The values at the constant q_t were also plotted in (b) as adsorption isotherms of equilibrium Sb concentration. It was noted that the adsorption amount of Sb followed in the order of APC-Ce 0.1 > APC-Ce 0.05 > APC-Ce 0.01 > APC-Ce 0.005 > APC. Nevertheless, the adsorption capacity of APC was approximately equivalent to PES-CeO_2. Notably, the values of q_e increased significantly with an increasing CeO_2 loading in the post-oxidated fibers. However, the CeO_2-PES fiber composite with higher CeO_2 loading resulted in a lower uptake value of Sb. This might be due to that CeO_2 distributed inside of the fiber. These data of the equilibrium adsorption isotherm and related isotherm parameters were analyzed using Langmuir and Freundlich models (Figure 5). In Langmuir models following equation to correlate adsorption equilibrium is used: $\frac{C_e}{q_e} = \frac{1}{q_m \times K} + \frac{C_e}{q_m}$ (4), where q_e is the amount of Sb adsorbed at equilibrium (mg/g), K is Langmuir constant and q_{max} is maximum adsorption capacity (mg/g), C_i and C are the initial and final concentration of the Sb in the solution (mg/L), and V represents the volume of the solutions (L). In Freundlich equation $lnq_e = lnK_f + \frac{1}{n} lnC_e$ (5), is used with K_F and n for Freundlich constants. These results indicated that the adsorption data obtained fit the Langmuir models well.

According to their analysis, the resulting parameters are listed in Table 2. The value of q_m for APC fiber was 4.2 mg/g, indicating that Al_2O_3 had the ability to adsorb Sb. Furthermore, the values of adsorption capacities at pH 6.0 for the APC-Ce 0.005 and APC-Ce 0.1, for the post-deposited CeO_2-Al_2O_3 composite fibers, were increased from 4.97 to 7.71 mg/g with increasing CeO_2 loading on the fiber. In contrast, the PES-CeO_2 fiber having higher contents of CeO_2 was 4.35 mg/g, indicating that CeO_2 loaded inside the fiber was not effectively involved in the adsorption. As seen in Table 3, those could be compared with other adsorbents for antimony. Among these adsorbents, the iron adsorbent used in the acidic dipping method had high q_m value with 17.9 mg/g, but APC-Ce 0.1 fiber in the present study had 7.7 mg/g, indicating its highly efficient adsorption capacity being next highest maximum adsorption.

3.3 Continuous flow column adsorption for antimony

The breakthrough curves, ratio of the initial Sb concentration C_o, and that at each time C_t was plotted at time as shown in Figure 6 (a). So, depicting the breakthrough curves for APC-Ce 0.05 fibers and APC fiber presents the effect of C_t/C_o on different column height of 10 cm, 20 cm, and 30 cm and different flow rates of 2.5 mL/min and 5 mL/min. Here the Sb concentration was 10 ppm at flow rate of 5.0 ml/min through breakthrough times. With increasing operation time, the C_t/C_o at each time for adsorption of antimony tended to saturate, approaching $C_t/C_o = 1$ for Figure 6 (b), where no adsorption occurred. It was found that as the column length increases, the operation time to reach this point tended to increase. This could be attributed to the longer contact time with the solution. Therefore, the contact time T_c was calculated from the following equation with column height H, radius column r, and water flow rate Q (mL/min): $T_c = \frac{1}{Q} \times \pi(\frac{r}{2})^2 H$ (6) [30]. When the column height was changed for 10 cm, 20 cm, and 30 cm, the T_c values calculated were 2.7 minutes, 5.3 minutes, and 8.0 minutes, respectively. As the

column height increased, the contact time of the water solution and the adsorbent increased proportionally, allowing for efficient adsorption to the fibers. Figure 6 (a) contains the results of APC-Ce 0.05 for 20 cm column at a flow rate of 2.5 mL/min. Clearly, the removal rate has improved over time. In this case, the contact time T_c is 10.6 minutes, indicating that the contact between the antimony and the fiber was more conductive to the separation than when the flow rate was 5 mL/min. Figure 6 (b) presents breakthrough curves obtained at a bed depth of 20 cm using APC-Ce 0.05 fiber, when varied initial concentrations of Sb in the range of 10, 15, and 20 mg/L. Notably, the breakthrough curves exhibited a steeper shape as the initial concentration of Sb increased. This indicated that the adsorption of Sb reached saturation more rapidly at higher initial concentrations. Furthermore, the experimental data was fitted using the Adams - Bohart model, which assumes a rectangle isotherm, and the calculation was performed using the equation $\frac{C_t}{C_o} = \frac{1}{1+\exp\left(k_{AB}N_o\frac{H}{Lv}-k_{AB}C_o t\right)}$ (7), where k_{AB} is kinetic constant of Adams – Bohart model (L.h/mg), H is column height (cm), N_o is adsorption capacity per unit volume of the column bed (mg/L) and L_v is the liner velocity (cm/h). The maximum adsorption capacities per adsorbent mass denoted as q_{AB} (mg/L), were determined using the equation: $q_{AB} = \frac{N_o \pi r^2 H}{1000M}$ (8), where M is the adsorbent mass (g). Table 4 lists their parameters of Adams – Bohart model for APC-Ce 0.05 and APC fiber to Sb removal. When used for the APC-Ce 0.05 fiber with varying column lengths to be long, the K_{AB} value exhibited a decrease, from 0.017 to 0.04 at observed at 10 cm to 30 cm, meaning that longer column requires longer contact time. This suggested that increasing the column length improved the accessibility of antimony-fiber contact. Comparing APC and APC – Ce 0.05, the latter had a K_{AB} value about one-fifth smaller, while the maximum adsorption capacity (q_{AB}) was increased by approximately 10 times in the 20 cm column. This suggested that the increase in the number of adsorption sites of CeO_2 scattered on the fiber

surface was also effective in Sb capture by column. Furthermore, when employing APC-Ce 0.05 fiber at different flow rates, the maximum adsorption capacity (q_{AB}) exhibited an upward trend as the flow rate decreased. The q_{AB} values were recorded at 2.07 mg/g for a flow rate of 5 mL/min and significantly increased to 13.53 mg/g at 2.5 mL/min, resulting in sufficient antimony (Sb) adsorption onto the composite fibers at a slow flow rate. Similarly, an increase in the initial concentration of Sb from 10 to 20 mg/L led to a decrease in the maximum adsorption capacity q_{AB} from 2.07 mg/g to 0.42 mg/g. This decline could be explained by rapid saturation of adsorption sites on the adsorbent material at higher initial concentrations.

4. Conclusion

This study described a novel antimony adsorbent with fibrous shape with deposition of CeO_2. The Al_2O_3-PES composite fibers were forming with wet spinning and then CeO_2 was deposited on the surface by post oxidative reaction when APC fibers were soaked in $CeCl_3$ and oxidized by H_2O_2. The CeO_2 deposited was mainly dispersed on the fiber surface. The behavior of antimony adsorption followed Langmuir type mechanism having q_m value was as high as 7.1-7.7 mg/g for the CeO_2-deposited APC fibers. In addition, continuous column adsorption experiments according to the Adams-Bohart model showed that the introduction of CeO_2 into the fiber increased the efficiency of adsorption.

Acknowledgment

The XRD measurement and SEM-EDS observation were performed at the Nagaoka University of Technology Analysis and Instrumentation Center. We thank members of the Nagaoka University of Technology Analysis and Instrumentation Center for technical assistance.

Conflicts of interest

The authors reported no declarations of interest.

References

[1] M. He, N. Wang, X. Long, C. Zhang, C. Ma, Q. Zhong, A. Wang, Y. Wang, A. Pervaiz, J. Shan, Antimony speciation in the environment: Recent advances in understanding the biogeochemical processes and ecological effects, Journal of Environmental Sciences. 75 (2019) 14–39. https://doi.org/https://doi.org/10.1016/j.jes.2018.05.023.

[2] I. Herath, M. Vithanage, J. Bundschuh, Antimony as a global dilemma: Geochemistry, mobility, fate and transport, Environmental Pollution. 223 (2017) 545–559. https://doi.org/https://doi.org/10.1016/j.envpol.2017.01.057.

[3] H. Tian, J. Zhou, C. Zhu, D. Zhao, J. Gao, J. Hao, M. He, K. Liu, K. Wang, S. Hua, A Comprehensive Global Inventory of Atmospheric Antimony Emissions from Anthropogenic Activities, 1995–2010, Environ Sci Technol. 48 (2014) 10235–10241. https://doi.org/10.1021/es405817u.

[4] S. Ishihara, T. Ohno, Present status of antimony mineral resource of this world, Shigen-Chishitsu. 62 (2012) 91–97. https://doi.org/10.11456/shigenchishitsu.62.91.

[5] M. Fort, J.O. Grimalt, X. Querol, M. Casas, J. Sunyer, Evaluation of atmospheric inputs as possible sources of antimony in pregnant women from urban areas, Science of The Total Environment. 544 (2016) 391–399. https://doi.org/https://doi.org/10.1016/j.scitotenv.2015.11.095.

[6] L. Bregoli, F. Chiarini, A. Gambarelli, G. Sighinolfi, A.M. Gatti, P. Santi, A.M. Martelli, L. Cocco, Toxicity of antimony trioxide nanoparticles on human hematopoietic progenitor cells and comparison to cell lines, Toxicology. 262 (2009) 121–129. https://doi.org/https://doi.org/10.1016/j.tox.2009.05.017.

[7] A. Periferakis, A. Caruntu, A.T. Periferakis, A.E. Scheau, I.A. Badarau, C. Caruntu, C. Scheau, Availability, Toxicology and Medical Significance of Antimony, Int J Environ Res Public Health. 19 (2022). https://doi.org/10.3390/ijerph19084669.

[8] China Antimony Industry Report, ResearchInChina. (2012) 46. http://www.researchinchina.com/htmls/report/2012/6351.html?fbclid=IwAR2qHlHkeGY5iCWiHczf7LpFZr8tvd6v_C1wXr581z0z7WUFR3h17bme67s (accessed June 9, 2023).

[9] D. Dupont, S. Arnout, P.T. Jones, K. Binnemans, Antimony Recovery from End-of-Life Products and Industrial Process Residues: A Critical Review, Journal of Sustainable Metallurgy. 2 (2016) 79–103. https://doi.org/10.1007/s40831-016-0043-y.

[10] X. Guo, Z. Wu, M. He, Removal of antimony(V) and antimony(III) from drinking water by coagulation–flocculation–sedimentation (CFS), Water Res. 43 (2009) 4327–4335. https://doi.org/https://doi.org/10.1016/j.watres.2009.06.033.

[11] Z. Wu, M. He, X. Guo, R. Zhou, Removal of antimony (III) and antimony (V) from drinking water by ferric chloride coagulation: Competing ion effect and the mechanism analysis, Sep Purif Technol. 76 (2010) 184–190. https://doi.org/https://doi.org/10.1016/j.seppur.2010.10.006.

[12] W. Xu, H. Wang, R. Liu, X. Zhao, J. Qu, The mechanism of antimony(III) removal and its reactions on the surfaces of Fe–Mn Binary Oxide, J Colloid Interface Sci. 363 (2011) 320–326. https://doi.org/https://doi.org/10.1016/j.jcis.2011.07.026.

[13] M.E.H. Bergmann, A.S. Koparal, Electrochemical antimony removal from accumulator acid: Results from removal trials in laboratory cells, J Hazard Mater. 196 (2011) 59–65. https://doi.org/https://doi.org/10.1016/j.jhazmat.2011.08.073.

[14] P.A. Riveros, The removal of antimony from copper electrolytes using amino-phosphonic resins: Improving the elution of pentavalent antimony, Hydrometallurgy. 105 (2010) 110–114. https://doi.org/https://doi.org/10.1016/j.hydromet.2010.08.008.

[15] P. Navarro, F.J. Alguacil, Adsorption of antimony and arsenic from a copper electrorefining solution onto activated carbon, Hydrometallurgy. 66 (2002) 101–105. https://doi.org/https://doi.org/10.1016/S0304-386X(02)00108-1.

[16] Y. Wang, X. Zhang, N. Ju, H. Jia, Z. Sun, J. Liang, R. Guo, D. Niu, H. Sun, High capacity adsorption of antimony in biomass-based composite and its consequential utilization as battery anode, Journal of Environmental Sciences. 126 (2023) 211–221. https://doi.org/https://doi.org/10.1016/j.jes.2022.05.050.

[17] B. Lapo, H. Demey, T. Carchi, A.M. Sastre, Antimony removal fromwater by a chitosan-iron(III)[ChiFer(III)] biocomposite, Polymers (Basel). 11 (2019). https://doi.org/10.3390/polym11020351.

[18] Y. Bai, F. Wu, Y. Gong, Oxidation and adsorption of antimony(iii) from surface water using novel Al2O3-supported Fe–Mn binary oxide nanoparticles: effectiveness, dynamic quantitative mechanisms, and life cycle analysis, Environ Sci Nano. 7 (2020) 3047–3061. https://doi.org/10.1039/D0EN00609B.

[19] L. Wang, J. Wang, Z. Wang, J. Feng, S. Li, W. Yan, Synthesis of Ce-doped magnetic biochar for effective Sb(V) removal: Performance and mechanism, Powder Technol. 345 (2019) 501–508. https://doi.org/https://doi.org/10.1016/j.powtec.2019.01.022.

[20] R. Yan, Z. Qiu, X. Bian, J. Yang, S. Lyu, A. Zhou, Effective adsorption of antimony from aqueous solution by cerium hydroxide loaded on Y-tape molecular sieve adsorbent: Performance and mechanism, Colloids Surf A Physicochem Eng

Asp. 604 (2020) 125317. https://doi.org/https://doi.org/10.1016/j.colsurfa.2020.125317.

[21] Z. Qi, T.P. Joshi, R. Liu, H. Liu, J. Qu, Synthesis of Ce(III)-doped Fe3O4 magnetic particles for efficient removal of antimony from aqueous solution, J Hazard Mater. 329 (2017) 193–204. https://doi.org/https://doi.org/10.1016/j.jhazmat.2017.01.007.

[22] A.G. Ilgen, T.P. Trainor, Sb(III) and Sb(V) Sorption onto Al-Rich Phases: Hydrous Al Oxide and the Clay Minerals Kaolinite KGa-1b and Oxidized and Reduced Nontronite NAu-1, Environ Sci Technol. 46 (2012) 843–851. https://doi.org/10.1021/es203027v.

[23] X. Guo, Z. Wu, M. He, X. Meng, X. Jin, N. Qiu, J. Zhang, Adsorption of antimony onto iron oxyhydroxides: Adsorption behavior and surface structure, J Hazard Mater. 276 (2014) 339–345. https://doi.org/https://doi.org/10.1016/j.jhazmat.2014.05.025.

[24] K. Nakamoto, M. Ohshiro, T. Kobayashi, Continuous flow column adsorption of mordenite zeolite–polymer compositfibers for lead removal, Desalination Water Treat. 109 (2018) 297–306. https://doi.org/10.5004/dwt.2018.22115.

[25] T. Kobayashi, M. Ohshiro, K. Nakamoto, S. Uchida, Decontamination of Extra-Diluted Radioactive Cesium in Fukushima Water Using Zeolite–Polymer Composite Fibers, Ind Eng Chem Res. 55 (2016) 6996–7002. https://doi.org/10.1021/acs.iecr.6b00903.

[26] K. Nakamoto, M. Ohshiro, T. Kobayashi, Mordenite zeolite—Polyethersulfone composite fibers developed for decontamination of heavy metal ions, J Environ Chem Eng. 5 (2017) 513–525. https://doi.org/https://doi.org/10.1016/j.jece.2016.12.031.

[27] K. Nakamoto, T. Kobayashi, Arsenate and arsenite adsorbents composed of nano-sized cerium oxide deposited on activated alumina, Sep Sci Technol. 54 (2019) 523–534. https://doi.org/10.1080/01496395.2018.1505914.

[28] K.S.W. Sing, Reporting physisorption data for gas/solid systems with special reference to the determination of surface area and porosity (Recommendations 1984), 57 (1985) 603–619. https://doi.org/doi:10.1351/pac198557040603.

[29] L. Nakajima, N.N.M. Yusof, T. Kobayashi, Calixarene-Composited Host–Guest Membranes Applied for Heavy Metal Ion Adsorbents, Arab J Sci Eng. 40 (2015) 2881–2888. https://doi.org/10.1007/s13369-015-1796-5.

[30] G. Nazari, H. Abolghasemi, M. Esmaieli, E. Sadeghi Pouya, Aqueous phase adsorption of cephalexin by walnut shell-based activated carbon: A fixed-bed column study, Appl Surf Sci. 375 (2016) 144–153. https://doi.org/https://doi.org/10.1016/j.apsusc.2016.03.096.

[31] C. Zhang, H. Jiang, Y. Deng, A. Wang, Adsorption performance of antimony by modified iron powder, RSC Adv. 9 (2019) 31645–31653. https://doi.org/10.1039/C9RA05646G.

[32] T. Yu, C. Zeng, M. Ye, Y. Shao, The adsorption of Sb(III) in aqueous solution by Fe2O3-modified carbon nanotubes, Water Science and Technology. 68 (2013) 658–664. https://doi.org/10.2166/wst.2013.290.

[33] E. Chmielewská, W. Tylus, M. Drábik, J. Majzlan, J. Kravčak, C. Williams, M. Čaplovičová, Ľ. Čaplovič, Structure investigation of nano-FeO(OH) modified clinoptilolite tuff for antimony removal, Microporous and Mesoporous Materials. 248 (2017) 222–233. https://doi.org/https://doi.org/10.1016/j.micromeso.2017.04.022.

[34] X. Zhao, X. Dou, D. Mohan, C.U. Pittman, Y.S. Ok, X. Jin, Antimonate and antimonite adsorption by a polyvinyl alcohol-stabilized granular adsorbent containing nanoscale zero-valent iron, Chemical Engineering Journal. 247 (2014) 250–257. https://doi.org/https://doi.org/10.1016/j.cej.2014.02.096.

[35] F. Shakerian, S. Dadfarnia, A.M. Haji Shabani, M. Nili Ahmad abadi, Synthesis and characterisation of nano-pore antimony imprinted polymer and its use in the extraction and determination of antimony in water and fruit juice samples, Food Chem. 145 (2014) 571–577. https://doi.org/https://doi.org/10.1016/j.foodchem.2013.08.110.

Table 1. Physical properties of Al_2O_3 powder and composite fibers.

	Al_2O_3 (wt%)	**Ce^{3+} concentration for post oxidation (M)**	**Ce content (wt%)**	**Density (cm^3/g)**	**Tensile strength (MPa)**	**BET surface area (m^2/g)**	**BJH pore volume (cm^3/g)**	**BJH pore size (nm)**
PES	-	-	-	0.79	9.5	58.8	0.718	4.26
PES-CeO_2	-	-	23.8	0.89	13.2	95.8	0.098	4.64
APC	60%	-	-	1.14	9.1	96.1	0.083	5.52
APC-Ce 0.005	60%	0.005	0.78	1.20	8.2	103.1	0.160	5.27
APC-Ce 0.01	60%	0.01	1.59	1.19	8.5	99.6	0.160	5.28
APC-Ce 0.05	60%	0.05	2.11	1.19	8.6	98.1	0.156	5.29
APC-Ce 0.1	60%	0.1	2.27	1.09	8.7	95.6	0.148	5.27

Table 2. Parameters of Langmuir and Freundlich analysis for Sb (III) adsorption with composite fibers.

	Langmuir model			**Freundlich model**		
	K_L	**q_m (mg/g)**	**R^2**	**K_F**	**n**	**R^2**
APC	3.0	4.2	0.979	1.5	2.3	0.996
APC-Ce 0.005	4.3	5.0	0.997	1.7	1.9	0.961
APC-Ce 0.01	5.7	6.3	0.999	2.2	1.8	0.944
APC-Ce 0.05	9.2	7.2	0.993	2.7	1.6	0.890
APC-Ce 0.1	8.0	7.7	0.982	2.9	1.7	0.835
PES-CeO_2	1.0	4.4	0.996	1.6	1.9	0.915

Table 3. Adsorption capacities of Sb (III) ion with using various adsorbents.

Adsorbent	**Synthetic method**	**Initial concentration (mg/L)**	**pH**	**Adsorption capacity (mg/g)**	**Reference**
Modified iron powder	Acid dipping method	20	5.0	17.9	[31]
Fe_2O_3 modified carbon nanotubes (CNTs)	Coagulation method	1.5	7.0	6.2	[32]
FeO(OH) zeolite	Sol-gel method	-	2.7	7.2	[33]
Nano-zerovalent iron stabilized by polyvinyl alcohol	Inverse suspension crosslinked method	0 – 20	7.0	7.0	[34]
Fe_2O_3 – Fe_3O_4/C prepared with bamboo template	Co-precipitation	5 – 150	7.0	4.8	[34]
Fe_2O_3 – Fe_3O_4/C prepared with eucalyptus wood template	Co-precipitation	50	8.0	4.5	[34]
Sb(III) imprinted sorbent	Sol-gel method	-	5.0	6.7	[35]
Al_2O_3-PES composite fiber	Water coagulation with wet spining	10	6.0	7.2	This work
CeO_2 alumina composite fibers	Al_2O_3-scafolding post oxidative deposition	10	6.0	7.7	This work

Table 4. Calculated parameter of Adams – Bohart model.

Adsorbent	H (cm)	Q (mL/min)	C_0 (mg/L)	K_{AB} (L.h/mg)	N_0 (mg/L)	q_{AB} (mg/g)	R^2
APC-Ce 0.05	10	5	10	0.017	195.1	0.61	0.86
	20	5	10	0.011	342.7	2.07	0.98
	20	2.5	10	0.005	2241.7	13.53	0.93
	30	5	10	0.004	849.1	7.68	0.90
	20	5	10	0.011	342.66	2.07	0.98
	20	5	15	0.010	277.14	1.67	0.92
	20	5	20	0.008	135.09	0.42	0.95
APC	20	5	10	0.050	57.65	0.18	0.77

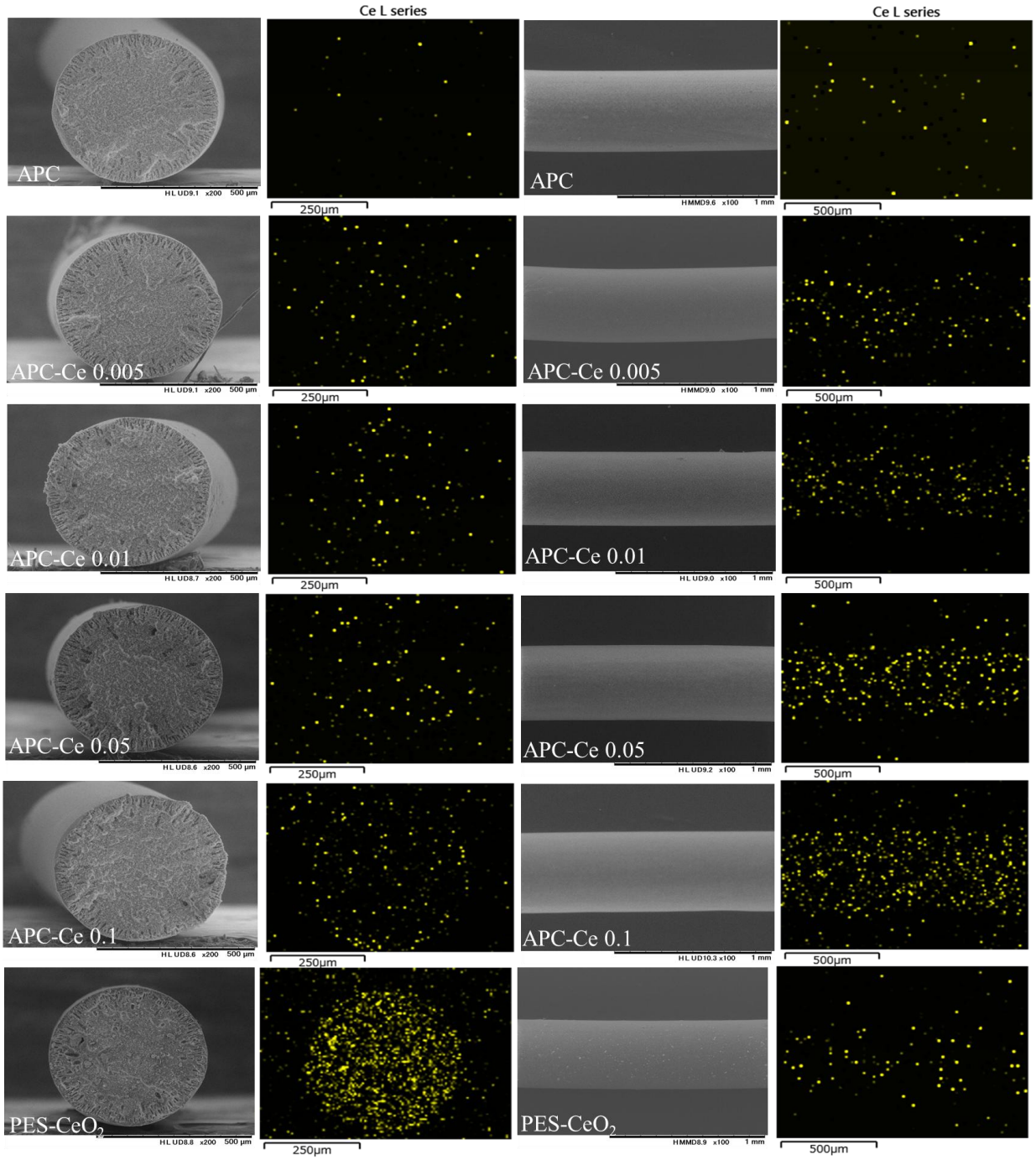

Figure 1. SEM morphology and EDS mapping of Ce for cross-section and surface of Al_2O_3 composite fibers deposited with CeO_2 and PES-CeO_2 fiber.

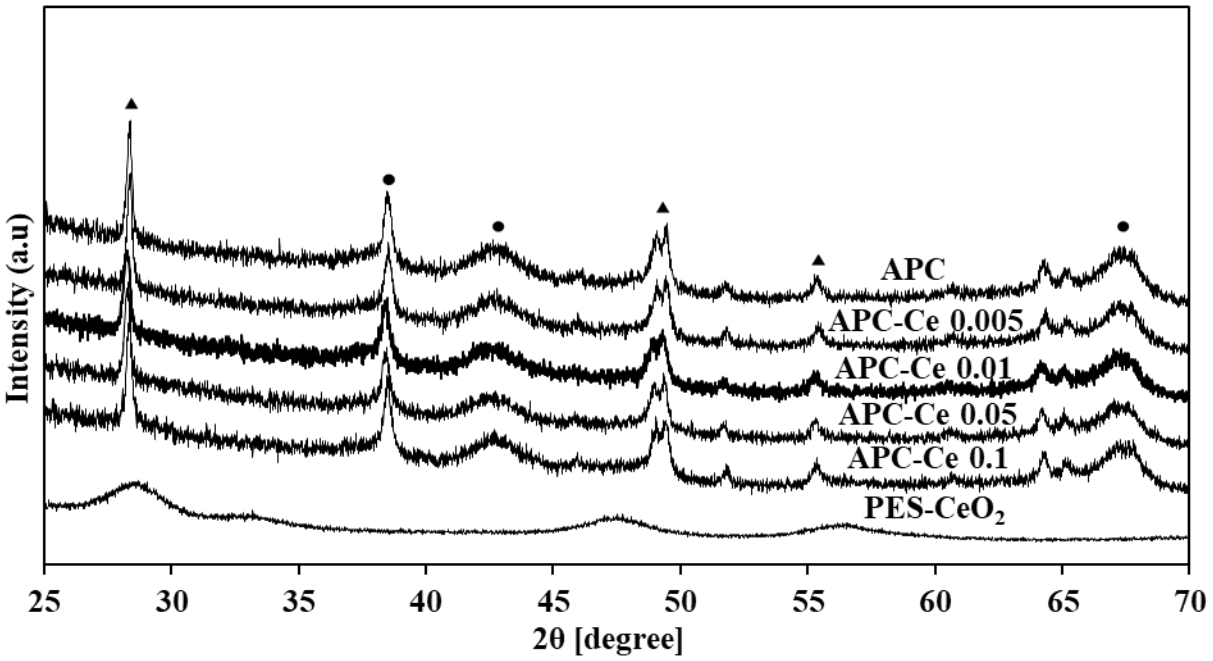

Figure 2. XRD patterns of Al_2O_3 composite fibers deposited with CeO_2 and PES-CeO_2 composite fiber (circle symbol (●) was assigned to x- Al_2O_3 and triangle symbol (▲) was for CeO_2).

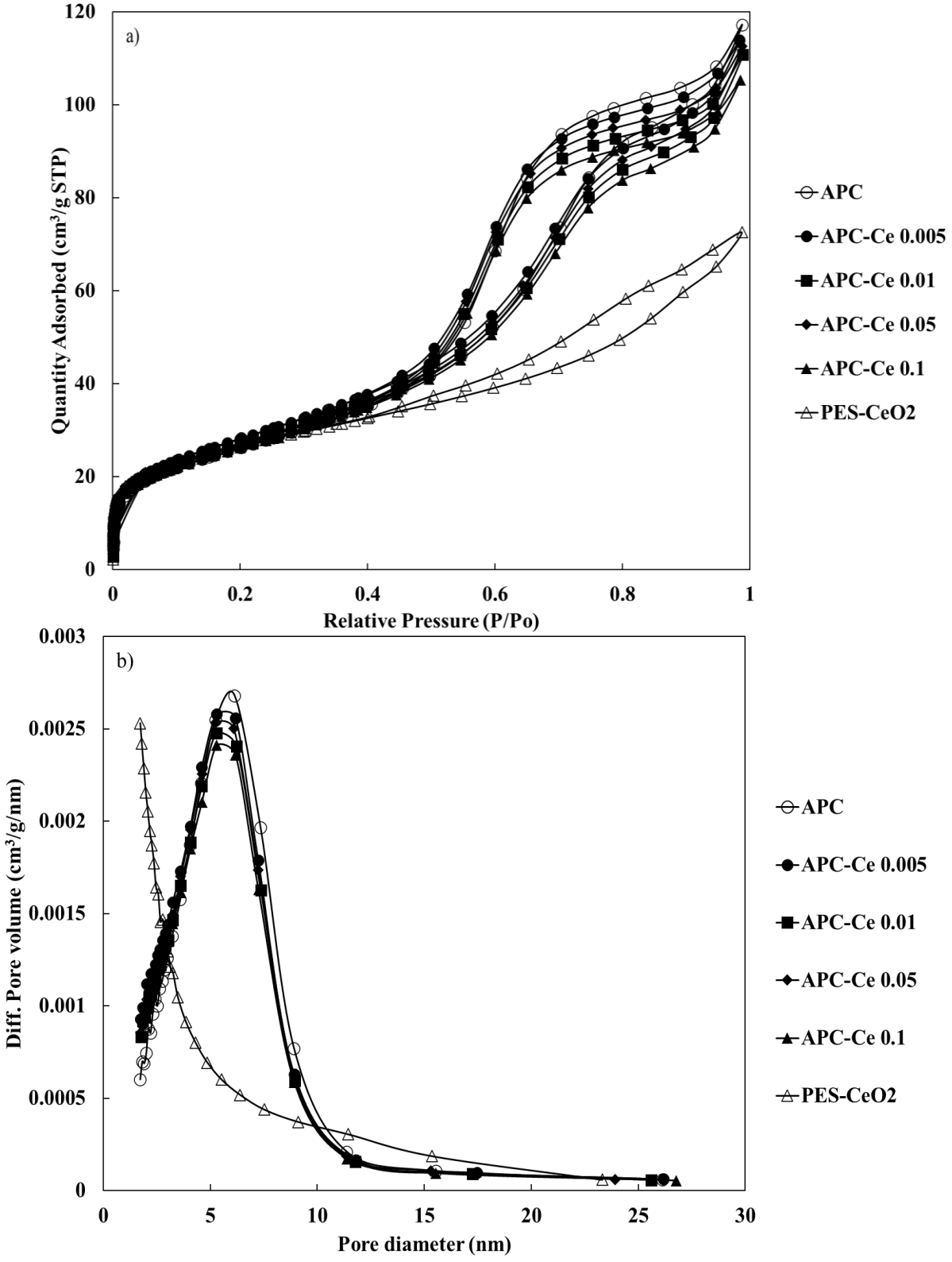

Figure 3. a) N_2 adsorption isotherm and b) BJH pore distribution of each fibers.

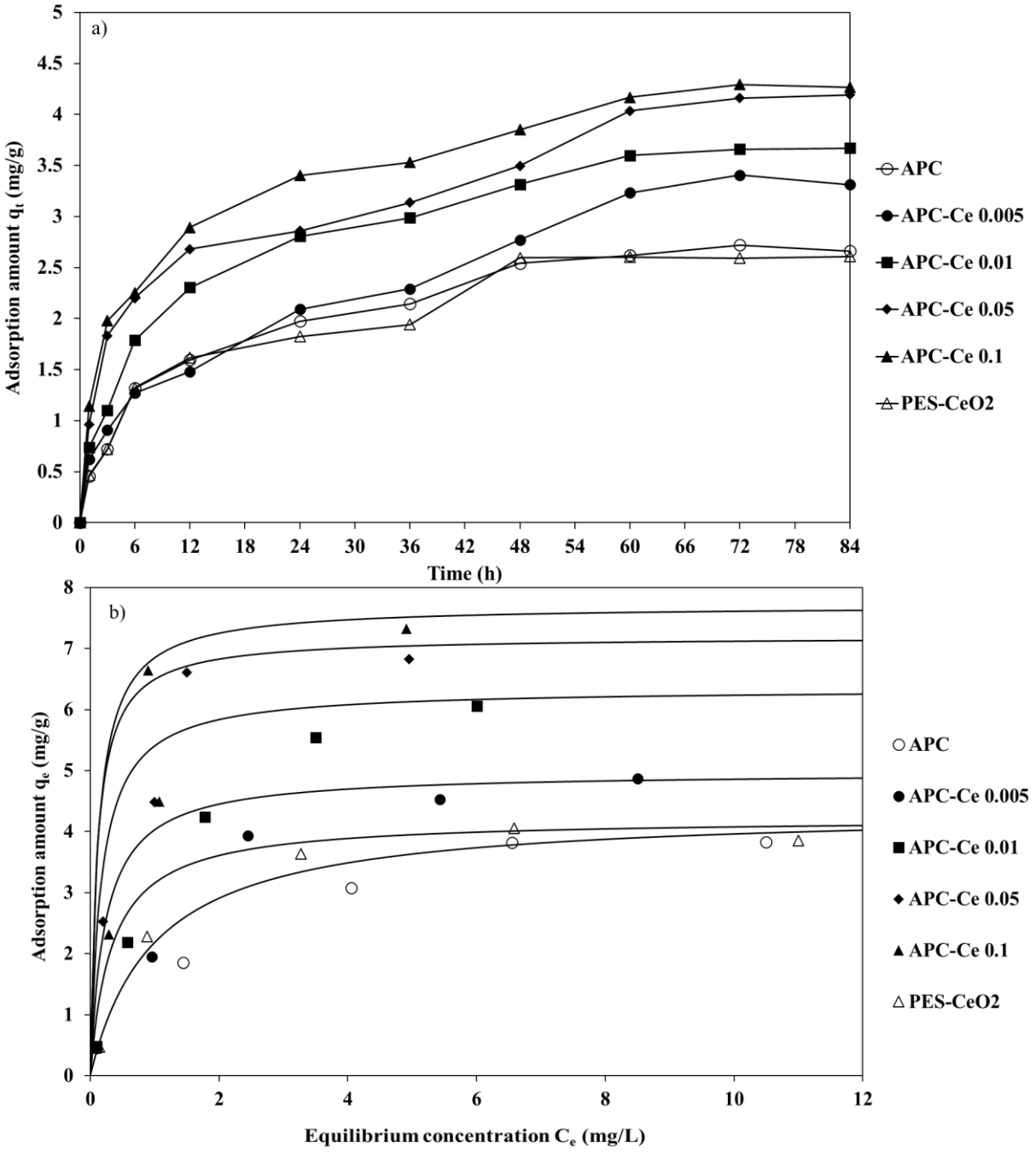

Figure 4. a) Time change of adsorption amount of antimony for the composite fibers and b) adsorption isotherms of Sb. The pH of aqueous solution was 6 and Sb concentration of a) was 10 mg/L**.**

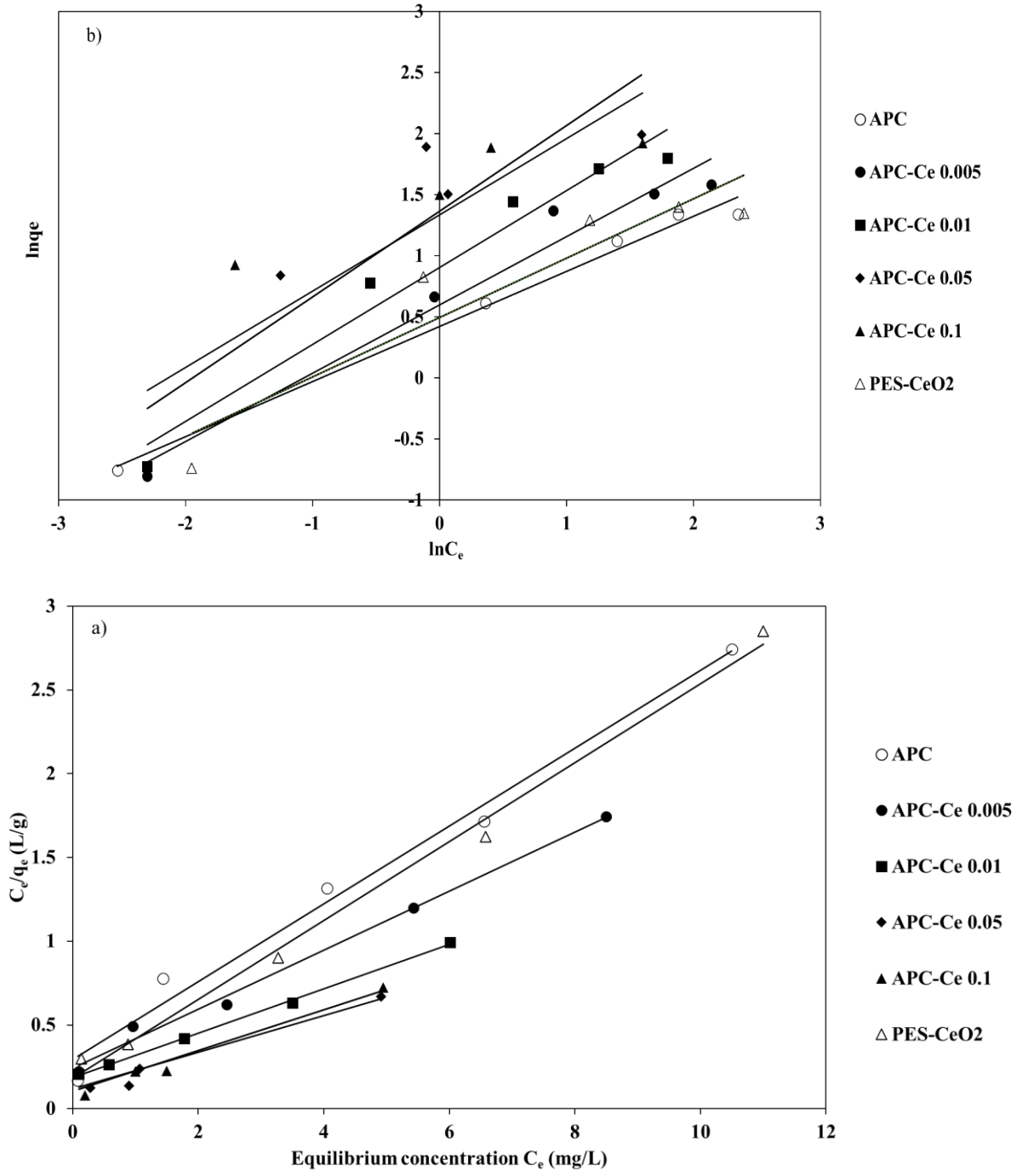

Figiure 5. a) Langmuir and b) Freundlich isotherm linear plots.

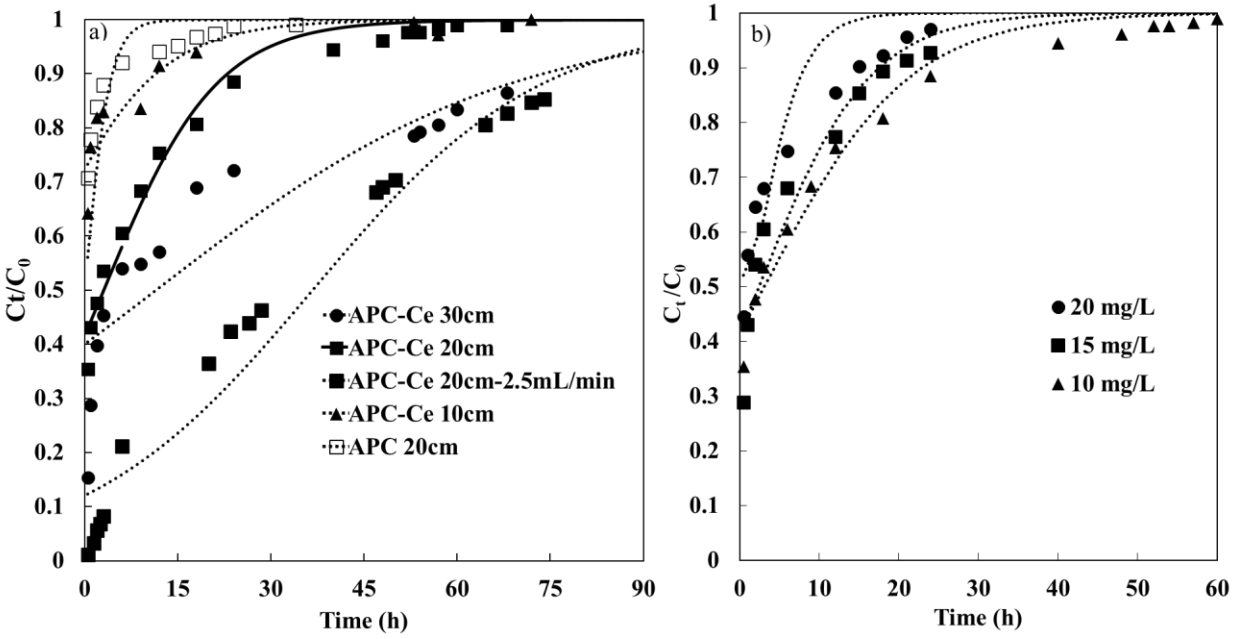

Figure 6. Adams – Bohart model breakthrough curve of Sb^{3+} at different a) bed height and b) initial Sb^{3+} concentration.